



# Performance of grape (*Vitis vinifera* L.) industrial processing solid waste–derived nanoporous carbon in copper(II) removal

Fuat Güzel<sup>1</sup> · Gülbahar Akkaya Saygılı<sup>1</sup> · Hasan Saygılı<sup>2</sup> · Filiz Koyuncu<sup>1</sup> · Nafiye Kaya<sup>1</sup> · Süreyya Güzel<sup>1</sup>

Received: 3 April 2020 / Revised: 18 May 2020 / Accepted: 20 May 2020 / Published online: 5 June 2020  
© Springer-Verlag GmbH Germany, part of Springer Nature 2020

## Abstract

In this study, copper removal performance of new nanoporous carbon adsorbent (grape waste nanoporous carbon (GWNC)) produced from industrial grape processing solid waste (grape waste) under optimized conditions was investigated. The optimization of removal conditions was determined by examining the effects of GWNC dosage, pH, initial Cu(II) concentration, contact time, and temperature. Kinetic and isotherm data were evaluated in pseudo-first-order and pseudo-second-order kinetic models and Langmuir, Freundlich, and Dubinin-Radushkevich isotherm models, respectively. Kinetic and isotherm data displayed that the Cu(II) adsorption onto GWNC can be well defined by the pseudo-second-order kinetic model and the Langmuir isotherm model. The diffusion mechanism of adsorption was explained using the intra-particle diffusion model. The Cu(II) removal capacity of GWNC at determined optimized conditions was determined to be 80.0 mg g<sup>-1</sup>. The calculated thermodynamic data revealed the spontaneous and endothermic nature of the Cu(II) adsorption. Desorption studies showed that H<sub>2</sub>SO<sub>4</sub> was the effective desorption agent with the desorption rate of 89.14%. The results in this study emphasized that GWNC is an alternative effective adsorbent to commercial adsorbents for Cu(II) removal.

**Keywords** Copper removal · Grape processing waste · Nanoporous carbon · Spectral analysis · Kinetics · Isotherm

## 1 Introduction

The heavy metals released from industrial activities such as mining, ore processing, fertilizer production, battery production, and pesticides and heavy metal processing, increasing demands with increasing population, are an important cause of pollution in soil and water resources [1]. They are very toxic and non-biodegradable. The pollution created by them in varied water resources is of major importance due to the toxic effect on humans and other living organisms in the ecosystem [2]. Copper is one of the commonly utilized heavy metal in the metallurgy, electroplating, pigment, plastic, and mining industry [3]. These industries produce a lot of wastewater and sludge containing various concentrations of Cu(II)

and having an unfavorable effect on the water medium [2]. It has been well reported that the aggregation of copper in the body of humans leads to headache, brain, anemia, skin, and heart illnesses. The permitted amount of copper in water is limited by 2.5 mg L<sup>-1</sup> [4]. Therefore, the removal of copper ions from polluted drinking water and wastewater is important for protecting living organisms.

Various methods like chemical precipitation, flotation, coagulation, ion exchange, adsorption, reverse osmosis, and electro dialysis are used to reduce the problem of copper-containing water pollution [4, 5]. However, most of these techniques other than adsorption limit their application due to high cost, secondary pollution, and inefficiency at low concentrations of Cu(II) (< 100 ppm) [6]. For this purpose, adsorption technology is used more frequently than other methods because it is cheap and easy to design [7]. Until now, many different adsorbents have been researched to identify low-cost and effective precursors and preparation methods for use in adsorption studies to remove copper ions in water. Among them, nanoporous carbon (NC) adsorbents are known to be highly efficient materials owing to their large porosity, high surface area, surface chemistry properties, and surface reactivity. Because of these properties, they provide the

✉ Fuat Güzel  
fguzel@dicle.edu.tr; guzelfast@gmail.com

<sup>1</sup> Department of Chemistry, Faculty of Education, Dicle University, 21280 Diyarbakır, Turkey

<sup>2</sup> Department of Petroleum and Natural Gas Engineering, Faculty of Engineering and Architecture, Batman University, 72100 Batman, Turkey

advantage of simultaneously removing inorganic and organic pollutants in wastewater treatment [8]. However, these materials are more costly than other adsorbents. Therefore, there has recently been increased interest in studies aimed at using renewable and low-cost precursors for NC production [9].

According to our knowledge, no studies have been found on the removal of Cu(II) from water by grape industrial processing solid waste-based nanoporous carbon. Grape (*Vitis vinifera* L.) is one of the most grown fruits in the world. Grape waste (GW) is one of the main food processing industry residues available worldwide since about 70 million tons of wine grape is produced annually. It is consumed raw and also used in the grape processing industry to produce by-products such as wine, juice, jam, and vinegar. Up to 20% of the harvested wine grape becomes waste during wine production [10]. According to the grape processing industry, about 0.3 kg of solid product is produced per kg of crushed grapes during production processes [11]. This waste originating from vineyard includes the skins, stalks, and grape seeds. These create various ecological hazards such as bad odors and surface and groundwater pollution [10]. To eliminate these effects, it is recommended as a raw material in industries such as pharmaceutical, cosmetics, feed, compost, and fertilizer [10, 12]. Therefore, alternative assessment methods are needed to protect the environment from these wastes and reintegrate them into the economy for reuse.

The main purpose of this research was to evaluate the feasibility of removing Cu(II) from the water-utilizing nanoporous material (grape water nanoporous carbon (GWNC)) fabricated from GW under water-optimized conditions with ZnCl<sub>2</sub> activation. Optimum copper adsorption conditions were decided by examining the effects of GWNC dosage, pH, initial Cu(II) concentration, contact time, and temperature on the Cu(II) adsorption performance of GWNC. In addition, kinetic, isotherm, and thermodynamic parameters of the Cu(II)-GWNC system were determined and discussed in detail. Also, to highlight the adsorption mechanism of copper, scanning electron microscopy/energy-dispersive X-ray spectroscopy (SEM-EDX), Fourier transform infrared (FT-IR), and X-ray photoelectron spectroscopy (XPS) analyses before and after adsorption of GWNC were compared. In addition, the efficiency of different desorbing agents was investigated to recover the Cu(II) ions adsorbed on the GWNC.

## 2 Experimental

### 2.1 Materials

GW was procured from a winery in Turkey and applied as a precursor in the production of the GWNC. The optimization of its production conditions was discussed in our previous research. Some of its physicochemical properties are given in Table 1 [13]. Cu(II) stock solution was prepared by

dissolving CuSO<sub>4</sub>·5H<sub>2</sub>O at analytical grade ( $M_w = 249.68$  g/mol, purity > 99%) in ultra-pure water. The pH was set using 0.1 M NaOH and HCl solution. The chemicals used were supplied by the Sigma-Aldrich Company (Ankara, Turkey) and used in analytical grade.

### 2.2 Equipment

Batch adsorption experiments were performed in a temperature-controlled orbital shaker (Daihan WSB-30, South Korea). The pH was adjusted by a portable pH meter (Hanna pH 211, Italy). Cu(II) ion concentrations before and after adsorption were analyzed with an atomic absorption spectrophotometer (AAS) (PerkinElmer AAnalyst 400, USA). To explain the adsorption mechanism of copper on the GWNC surface, SEM-EDX, FT-IR, and XPS analyses were performed to examine the elemental composition of the main functional groups, the chemical condition, and their changes before and after Cu(II) adsorption on the GWNC surface. The morphology and elemental composition were visualized using scanning electron microscopy (SEM) (Zeiss, Germany) equipped with energy-dispersive X-ray spectroscopy (EDX) (Bruker, Germany). The functional groups were analyzed using an FT-IR spectrometer (PerkinElmer Spectrum 100, USA) in the range of 4000–400 cm<sup>-1</sup> at 4 cm<sup>-1</sup> resolution and 20 scans min<sup>-1</sup>. The elemental composition and chemical state on the surface were determined by using an XPS spectrometer (Thermo Scientific K-Alpha) with an Al K $\alpha$  monochromatized source.

**Table 1** Some physical and chemical properties of GWNC [13]

Properties	Values
Textural characteristics	
$S_{BET}$ (m <sup>2</sup> g <sup>-1</sup> )	1455
$V_{tot}$ (cm <sup>3</sup> g <sup>-1</sup> )	2.32
$V_{mic}$ (cm <sup>3</sup> g <sup>-1</sup> )	0.13
$V_{mes}$ (cm <sup>3</sup> g <sup>-1</sup> ) <sup>a</sup>	2.19
$V_{mic}$ (%)	5.39
$V_{mes}$ (%)	94.61
$D_p$ (nm)	6.81
Surface chemical characteristics	
Carboxylic (mEq g <sup>-1</sup> )	0.55
Phenolic (mEq g <sup>-1</sup> )	0.17
Lactonic (mEq g <sup>-1</sup> )	0.51
Acidity (mEq g <sup>-1</sup> )	1.23
Basicity (mEq g <sup>-1</sup> )	0.88

$S_{BET}$  is the BET surface area,  $V_{tot}$  is the total pore volume,  $V_{mic}$  is the micropore volume,  $V_{mes}$  is the mesopore volume,  $V_{mic}$  (%) is the microporosity,  $V_{mes}$  (%) is the mesoporosity, and  $D_p$  is the average pore diameter

<sup>a</sup> By difference

## 2.3 Adsorption and desorption of copper(II)

Cu(II) adsorption and desorption experiments were performed in a 100-mL Erlenmeyer flask comprising 50 mL of Cu(II) solution in a temperature-controlled orbital shaker set at 120 rpm shaking speed and desired temperature.

The impact of varied key parameters, such as pH (2.0–6.0), GWNC dose (50–100 mg), the initial Cu(II) concentration (100–400 mg L<sup>-1</sup>), contact time (5–480 min), and temperature (20–50 °C), was investigated by keeping other parameters constant. After each adsorption process, the adsorbent was separated from the solution by a 5000 rpm centrifugation rate for 10 min and the remaining metal ion concentrations were determined by an AAS apparatus. The experiments were carried out in triplicate under similar conditions, and the values were averaged. The adsorbed amount ( $q_t$ , mg g<sup>-1</sup>) at  $t$  time (min) and the amount of Cu(II) added at adsorbed equilibrium ( $q_e$ ) were calculated as follows:

$$q_t = \frac{(C_0 - C_t)V}{m} \quad (1)$$

$$q_e = \frac{(C_0 - C_e)V}{m} \quad (2)$$

where  $C_0$ ,  $C_t$ , and  $C_e$  (mg L<sup>-1</sup>) are the Cu(II) concentrations at initial time,  $t$  time, and equilibrium, respectively.  $V$  (l) is the volume of the solution, and  $m$  (g) is the amount of GWNC.

Desorption and reusability experiments were done with varied desorbing reagents such as HCl, HNO<sub>3</sub>, H<sub>2</sub>SO<sub>4</sub>, H<sub>3</sub>PO<sub>4</sub>, CH<sub>3</sub>COOH, C<sub>2</sub>H<sub>6</sub>O, C<sub>6</sub>H<sub>8</sub>O<sub>7</sub>, and H<sub>2</sub>O. To this end, for each eluent, GWNC was loaded with Cu(II) ions under optimized removal conditions. The 100 mg of GWNC loaded with Cu(II) ions was then transferred to a 50-mL Erlenmeyer flask containing 0.1 M of desorbing agent in 100-mL flasks. The metal-loaded adsorbents were agitated for 24 h at 298 K and 200 rpm. Then, the desorbed metal concentration was determined as mentioned before. Desorption efficiency (DE, %) was determined using the following equation:

$$DE(\%) = \frac{q_d}{q_a} \cdot 100 \quad (3)$$

where  $q_a$  and  $q_d$  (mg/g) are the adsorbed and desorbed amounts of adsorbate, respectively.

## 3 Results and discussion

### 3.1 Optimization of Cu(II) adsorption conditions

#### 3.1.1 Effect of pH

The pH value is one of the parameters that have the greatest effect on the adsorption process from solution, since it affects

properties of both adsorbent and adsorbate, such as surface charge, ionization degree, and chemical speciation [14]. This study was conducted on the basis of the speciation scheme for copper in the water reported in a previous study [15]. According to this scheme, at pH values above and below 6.0, copper exists in Cu(II) and Cu(OH)<sub>2</sub> ion state, respectively. Therefore, the influence of pH on experiments on Cu(II) removal by GWNC was explored in the pH 2.0–6.0 range and is presented in Fig. 1 a. From this figure, it is understood that the adsorbed amount of Cu(II) rises rapidly from pH 2.0 to pH 5.0 and then decreases very slightly. The reason for the low adsorption at low pH may be due to either the decrease of the active centers as a result of the protonation of the GWNC surface by the H<sup>+</sup> ions present in large amounts in the acidic medium or from the competitiveness of H<sup>+</sup> and Cu(II) for adsorption on the surface. On the contrary, the increase in the quantity of adsorbed Cu(II) by the increased pH is owing to the increase in the negatively charged centers, where the Cu(II) ions can be adsorbed and formed as a result of increased proton removal on the adsorptive surface with increasing pH, as noted by Jiang et al. [16]. For this reason, the optimal pH in this study was chosen as 5.0 for subsequent experiments.

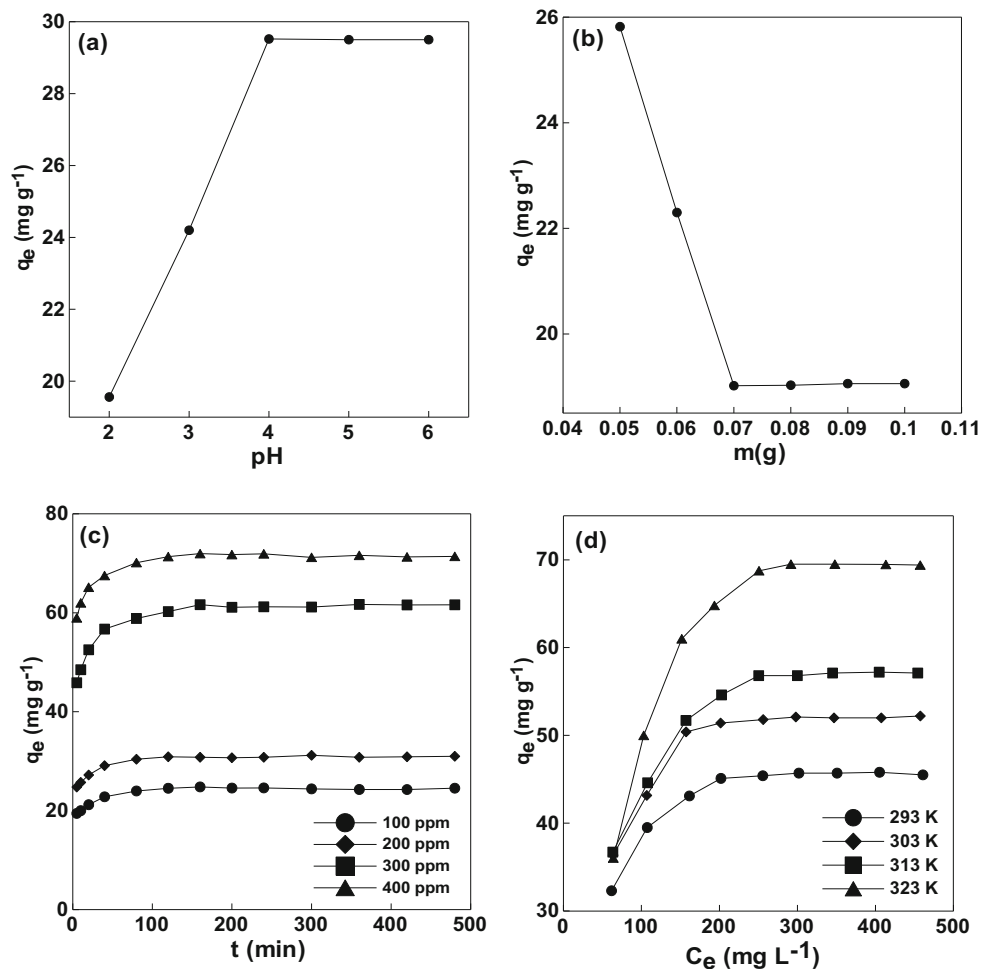
#### 3.1.2 Effect of GWNC dosage

The influence of GWNC dose on the removal of Cu(II) is demonstrated in Fig. 1 b. It is noticed from the figure that the amount of Cu(II) adsorbed decreases with the rise in the adsorbent mass. This decrease is probably owing to the decrease in the availability of active adsorption centers and surface area due to the overlapping or clustering aggregation of the adsorbent surface with increasing adsorbent dosage, as noted by Zhang et al. [17]. As a result, the optimal adsorbent dosage was selected to be 50.0 mg for the following experiments.

#### 3.1.3 Effect of initial copper concentration/contact time

Figure 1 c shows the influence of contact time/initial concentration on the Cu(II) adsorption by GWNC. It is observed from this figure that the amount of adsorbed Cu(II) increases quickly in the initial 45 min and reaches equilibrium in 120 min. This phenomenon can be attributed to the rapid increase in the metal amount adsorbed in the first step, the existence of various adsorptive centers and functional groups on the adsorbent surface [18]. Therefore, the optimum contact time for isotherm experiments was chosen as 120 min. It also shows that the adsorbed amount increased with an increase of the initial Cu(II) concentration from 100 to 400. This may possibly be caused by increased interaction with the surface due to the increased mass transfer driving force of ions to the surface

**Fig. 1** Effects of solution pH (a), adsorbent dose (b), initial Cu(II) concentration and contact time (c), and solution temperature (d) on the adsorption of Cu(II) onto GWNC



and pores of the adsorbent with increased Cu(II) concentration.

### 3.1.4 Effect of temperature

Figure 1 d displays the temperature influence on the Cu(II) adsorption by GWNC. It can be noticed that the adsorbed quantity of Cu(II) increases with rising temperature from 20 to 50 °C, implying that the process is endothermic in nature. This increase can be caused by the ease in the orientation of the Cu(II) ions to the adsorbent surface due to the reduction in the thickness of boundary layer surrounding the adsorbent with the increase in temperature [19].

### 3.2 Kinetic modeling

For kinetic modeling, kinetic data in Fig. 1 c were evaluated in commonly used pseudo-first-order [20] and pseudo-second-order [21] kinetic models. The linear equation of these models is expressed as follows:

Pseudo-first-orderkinetic model :  $\log(q_e - q_t)$

$$= \log q_e - \frac{k_1}{2.303} t \quad (4)$$

Pseudo-second-orderkinetic model :  $\frac{t}{q_t} = \frac{1}{k_2 q_e^2} + \frac{t}{q_e}$  (5)

where  $k_1$  (min<sup>-1</sup>) and  $k_2$  (g mg<sup>-1</sup> min<sup>-1</sup>) are rate constants of pseudo-first-order and pseudo-second-order kinetic models, respectively. The most appropriate kinetic model was chosen according to the compatibility between the experimental adsorbed amount ( $q_{e,exp}$ ) and the calculated adsorbed amount ( $q_{e,cal}$ ), linear regression correlation coefficients ( $R^2$ ), and normalized standard deviation ( $\Delta q$  (%)) values for kinetic data at different initial concentrations. The  $\Delta q$  (%) values were calculated from this equation

$$\Delta q(\%) = \sqrt{\frac{\sum_{i=1}^N \left( \frac{q_{e,exp} - q_{e,cal}}{q_{e,exp}} \right)^2}{N-1}} \times 100 \quad (6)$$

where  $N$  is the number of data points.

The values of kinetic parameters ( $R^2$  and  $\Delta q$  (%)) of both models were calculated using the intercept and slope values obtained from the graphs (not shown) of  $\ln(q_t - q_e)$  vs.  $t$  and of  $t/q_t$  vs.  $t$ , respectively, and are listed in Table 2. It can be seen from the table that the pseudo-second-order model for initial Cu(II) concentrations studied has the highest  $R^2$  value ( $> 0.9989$ ) and the lowest  $\Delta q$  (%) value ( $< 0.40$ ) than the pseudo-first-order model. In addition, it is seen from the table that the  $q_{e,cal}$  values determined for the pseudo-second-order model are closer to the  $q_{e,exp}$  than the  $q_{e,cal}$  values determined from the pseudo-first-order model. These facts indicate that the kinetics of the GWNC-Cu(II) adsorption system at various initial concentrations studied is defined by the pseudo-second-order model.

### 3.3 Diffusion mechanism

To explain the diffusion mechanism and rate-controlling steps that affect the Cu(II) adsorption onto GWNC, kinetic data in Fig. 1 c were evaluated in the equation of the theory-based intra-particle diffusion model proposed by Weber and Morris [22]. The mathematical representation of this model is expressed as

$$q_t = k_{id}t^{1/2} + I \tag{7}$$

where  $k_{id}$  ( $\text{mg g}^{-1} \text{min}^{-1/2}$ ) is the intra-particle diffusion rate constant and  $I$  ( $\text{mg g}^{-1}$ ) is the thickness of the boundary layer.  $I$  value is close to 0 means that the only rate control step of the adsorption process is diffusion [23]. According to this model,

if intra-particle diffusion exists in an adsorption phenomenon and also is the only rate-limiting stage, the plot of  $q_t$  vs.  $t^{1/2}$  line passes through the origin. When the plot does not pass through the origin, this means that the intra-particle diffusion is not the only rate-controlling stage, and also other kinetic models may simultaneously control the adsorption rate [24, 25].

The intra-particle diffusion plots of Cu(II) adsorption onto GWNC are displayed in Fig. 2. The graph has three stages over the entire time range, and with it, the plots do not pass through the origin implying that intra-particle diffusion is not solely rate-limiting step and the boundary layer also affects the adsorption process. As a result, these facts imply that the Cu(II) adsorption by GWNC is a complex process involving multiple mechanisms. The  $k_{id}$  and  $I$  constants for this model were calculated from the slope and intercept of the linear second part of the graphs in Fig. 2, respectively, and are given in Table 2. From the table,  $I$  values are greater than 0 and increase with a rise in initial concentration. This fact also confirms that the rate controlling of Cu(II) adsorption by GWNC affects not only the intra-particle diffusion step but also the diffusion in the boundary layer.

### 3.4 Isotherm modeling

For isotherm modeling of GWNC-Cu(II) adsorption system, isotherm data in Fig. 1 d were evaluated in the linear equations of widely used Langmuir [26], Freundlich [27], and Dubinin-Radushkevich (D-R) [28] isotherm models. The mathematical expressions of these isotherm models are

$$\text{Langmuir : } \frac{C_e}{q_e} = \frac{1}{q_m b} + \frac{1}{q_m} C_e \tag{8}$$

$$\text{Freundlich : } \ln q_e = \ln K_F + \frac{1}{n_F} \ln C_e \tag{9}$$

$$\text{D-R : } \ln q_e = \ln q_D - \left( \frac{RT}{\sqrt{2}E} \right)^2 \cdot \left( \ln \left( 1 + \frac{1}{C_e} \right) \right)^2 \tag{10}$$

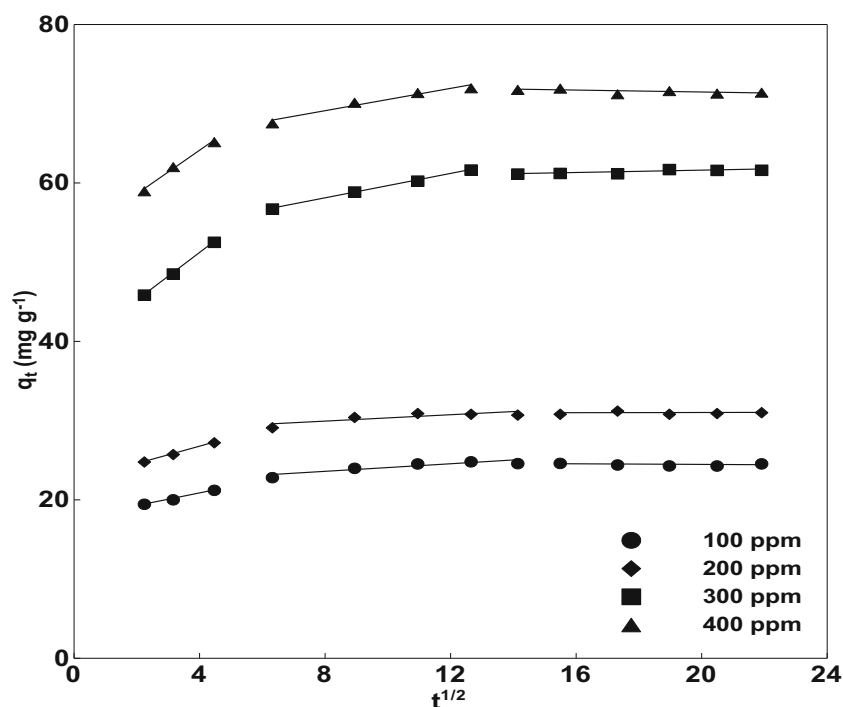
where  $q_m$  ( $\text{mg g}^{-1}$ ) is the Langmuir maximum adsorption capacity of adsorbent,  $b$  ( $\text{L mg}^{-1}$ ) is the Langmuir constant related to the adsorption equilibrium, and  $K_F$  ( $(\text{mg g}^{-1}) (\text{L mg}^{-1})^{1/n}$ ) and  $n$  are Freundlich constants which are the measure of adsorbent capacity and adsorption intensity, respectively.  $q_{D-R}$  ( $\text{mg/g}$ ) is the D-R maximum adsorption capacity of adsorbent, and  $E$  ( $\text{J mol}^{-1}$ ) is the mean energy of adsorption per molecule of the adsorbate. The most suitable model was determined according to  $R^2$  and  $\Delta q$  (%) values.

$R_L$ , the dimensionless separation factor, is usually used to evaluate the adsorption feasibility and was calculated using Eq. (11). The value of  $R_L$  indicates irreversible ( $R_L = 0$ ), favorable ( $0 < R_L < 1$ ), and linear ( $R_L = 1$ ) adsorptions or unfavorable adsorption ( $R_L > 1$ ) [29].

**Table 2** Kinetic parameters for Cu(II) adsorption onto GWNC

	$C_0$ ( $\text{mg L}^{-1}$ )			
	100	200	300	400
$q_{e,exp}$ ( $\text{mg g}^{-1}$ )	24.50	30.88	61.42	71.58
Pseudo-first order				
$q_{e,cal}$ ( $\text{mg g}^{-1}$ )	6.07	7.35	14.72	12.74
$k_1 \times 10^{-2}$ (1/min)	3.16	3.52	2.16	2.76
$R^2$	0.9983	0.9997	0.9760	0.9872
$\Delta q$ (%)	6.12	4.52	4.82	3.92
Pseudo-second order				
$q_{e,cal}$ ( $\text{mg g}^{-1}$ )	23.53	30.03	61.35	71.43
$k_2 \times 10^{-3}$ ( $\text{g mg}^{-1} \text{min}^{-1/2}$ )	27.10	22.10	6.00	8.60
$R^2$	0.9989	0.9992	0.9998	0.9998
$\Delta q$ (%)	0.40	0.35	0.25	0.27
Intra-particle diffusion				
$C$ ( $\text{mg g}^{-1}$ )	20.93	27.59	51.87	63.38
$k_{id}$ ( $\text{mg mg}^{-1} \text{min}^{-1/2}$ )	0.32	0.28	0.71	0.77
$R^2$	0.9579	0.9394	0.9988	0.9582
$\Delta q$ (%)	0.47	0.72	0.21	0.34

**Fig. 2** Intra-particle diffusion kinetic plots for the adsorption of Cu(II) at different initial concentrations onto GWNC



$$R_L = \frac{1}{1 + q_m C_0} \quad (11)$$

The parameters of Freundlich, Langmuir, and D-R isotherm models were determined from the intercept and slope of the plots (not shown) of  $\ln q_e$  vs.  $\ln C_e$ ,  $1/q_e$  vs.  $1/C_e$ , and  $\ln q_e$  vs.  $\ln [(1 + 1/C_e)]^2$ , respectively, and are listed in Table 3. It is observed from the table that the Langmuir isotherm model best defines the GWNC-Cu(II) adsorption system since it has the highest  $R^2$  values ( $> 0.9907$ ) and the lowest  $\Delta q$  (%) values ( $< 0.55$ ) at all temperatures. As it is noticed from Table 3, the  $q_m$  and  $b$  Langmuir constants increase with temperature, implying that the adsorption intensity is higher at higher temperatures and that the process is endothermic. Also, this table shows that maximum Cu(II) adsorption capacity determined from the Langmuir linear isotherm of GWNC is  $80.0 \text{ mg g}^{-1}$  at a solution pH value of 5.0, GWNC dosage of  $50.0 \text{ mg}$ , and temperature of  $50 \text{ }^\circ\text{C}$ . This high Cu(II) removal value of GWNC depends not only on its surface chemical property but also on the pore structure. The mesoporosity and mean pore diameter of GWNC are  $94.61\%$  and  $6.81 \text{ nm}$  (Table 1), respectively, and the ionic radius of copper is  $0.073 \text{ nm}$  [30]. These data clearly show that Cu(II) ions can easily penetrate into the pores of GWNC, causing its high adsorption. Table 4 lists a comparison of GWNC maximum Cu(II) adsorption capacity with other adsorbents that exist in the literature [31–39]. This table shows that GWNC has a Cu(II) adsorption capacity comparable to some adsorbents reported in the literature and is a potential and promising adsorbent. The  $R_L$  values in the range of  $0.0$ – $1.0$  at  $20$ – $50 \text{ }^\circ\text{C}$  verify the favorable

adsorption of Cu(II) onto GWNC. It was also observed that these values decreased with increasing adsorption

**Table 3** Isotherm and thermodynamic parameters for Cu(II) adsorption onto GWNC

	$T$ (K)			
	293	303	313	323
Langmuir				
$q_m$ ( $\text{mg g}^{-1}$ )	47.85	56.50	62.11	80.00
$b$ ( $\text{L mg}^{-1}$ )	0.0500	0.0363	0.0283	0.0179
$R^2$	0.9979	0.9979	0.9965	0.9907
$\Delta q$ (%)	0.22	0.36	0.40	0.55
$R_L$	0.1225	0.0812	0.0644	0.0476
Freundlich				
$K_F$ ( $(\text{mg g}^{-1}) (\text{L mg}^{-1})^{1/n}$ )	19.01	18.61	16.20	11.58
$1/n$	0.1505	0.1788	0.2165	0.3088
$R^2$	0.7824	0.8336	0.8497	0.8241
$\Delta q$ (%)	9.02	12.42	11.96	14.45
D-R				
$q_{D-R}$ ( $\text{mg g}^{-1}$ )	45.71	52.78	56.97	70.15
$E$ ( $\text{kJ mol}^{-1}$ )	0.05	0.04	0.04	0.03
$R^2$	0.9819	0.9580	0.9532	0.9821
$\Delta q$ (%)	6.32	8.10	8.45	6.01
Thermodynamic parameters				
$\Delta G^\circ$ ( $\text{kJ mol}^{-1}$ )	-0.964	-1.439	-1.810	-2.159
$\Delta H^\circ$ ( $\text{kJ mol}^{-1}$ )	10.90			
$\Delta S^\circ$ ( $\text{J mol}^{-1} \text{ K}^{-1}$ )	50.64			

**Table 4** Comparison of the maximum adsorption capacity of various adsorbents for Cu(II) ion removal

Adsorbents	$q_m$ (mg g <sup>-1</sup> )	pH	$T$ (K)	Reference
Grape bagasse carbon	43.47	5.0	318	[3]
Natural zeolite	8.97	6.0	303	[31]
Kaolinite	10.79	5.0	298	[32]
$\gamma$ -Al <sub>2</sub> O <sub>3</sub>	3.52	6.0	298	[33]
Rice husk carbon	25.25	5.0	313	[34]
Date stone carbon	31.25	6.0	293	[35]
Carbon nanotube	28.49	5.0	298	[36]
Commercial granular carbon	5.12	5.0	303	[37]
Commercial powder carbon	4.48	5.0	303	[37]
<i>Spartina alterniflora</i> biochar	48.49	6.0	298	[38]
Muskmelon peel biochar	78.74	7.0	303	[39]
GWNC	80.00	5.0	323	Present study

temperature, which confirms that the adsorption of Cu(II) is favorable for higher temperatures. This is also confirmed by the fact that the values of  $1/n$  in Table 3 determined from the Freundlich linear isotherms at studied temperatures are less than 1.0. In addition, the  $E$  values obtained by evaluating the equilibrium data in the D-R isotherm model give information about the physical or chemical properties of the process. The adsorption behavior is attributed to physical when  $E$  value is between 1.0 and 8.0 kJ mol<sup>-1</sup>, but to chemical when it is higher than 8.0 kJ mol<sup>-1</sup> [40]. As seen in Table 3, the  $E$  values determined at all temperatures studied were found to be < 8 kJ/mol, which indicates that adsorption occurs physically.

### 3.5 Thermodynamic evaluation

The thermodynamic behavior of the GWNC-Cu(II) system was explained by thermodynamic parameters comprising free energy ( $\Delta G^\circ$ , kJ mol<sup>-1</sup>), mean enthalpy ( $\Delta H^\circ$ , kJ mol<sup>-1</sup>), and mean entropy ( $\Delta S^\circ$ , J mol<sup>-1</sup> K<sup>-1</sup>). These parameters were calculated by evaluating the  $q_m$  and  $b$  values obtained from the linear Langmuir isotherms drawn according to the isotherm data obtained at the studied temperatures in the following equations, and these parameters given in Table 3.

$$K = q_m b \quad (12)$$

$$\Delta G^\circ = -RT \ln K \quad (13)$$

$$\ln K = -\frac{\Delta H^\circ}{RT} + \frac{\Delta S^\circ}{R} \quad (14)$$

where  $K$  is the adsorption equilibrium constant,  $R$  (8.314 J mol<sup>-1</sup> K<sup>-1</sup>) is the universal gas constant, and  $T$  (K) is the absolute temperature.

The negative  $\Delta G^\circ$  values (-0.964, -1.439, -1.810, and -2.159 kJ mol<sup>-1</sup> at 20, 30, 40, and 50 °C, respectively)

displayed that the Cu(II) adsorption process by GWNC was applicable and spontaneous. Further, the values of  $\Delta G^\circ$  with rising temperature are more negative, which confirms that the process is more favorable at high temperature and is endothermic. The endothermic character of the process was verified by a positive  $\Delta H^\circ$  (10.90 kJ mol<sup>-1</sup>) value. The positive  $\Delta S^\circ$  (50.64 J mol<sup>-1</sup> K<sup>-1</sup>) value showed increased randomness, which showed good affinity between the GWNC surface and Cu(II) during the adsorption process.

### 3.6 Spectral analysis of Cu(II) adsorption on GWNC

#### 3.6.1 SEM-EDX

The SEM and the corresponding EDX images of GWNC before and after adsorption are reported in Fig. 3 a and b. As shown in Fig. 3 a, the surface of the GWNC exhibited widely distributed porous surface structure, which suggested a greater potential to uptake Cu(II) ions [41]. After adsorption (Fig. 3b), a substantial alteration in the morphology of the surface has occurred, probably owing to the interaction of metal ions with the functional groups on the surface of porous carbon [42]. According to EDX results, before adsorption, the major elements on the surface of the material are carbon and oxygen. After the adsorption process, the appearance of new peaks for copper indicates the adsorption of Cu(II) ions on the GWNC surface [43]. Thus, the SEM-EDX analysis confirms that the GWNC has an ability to remove metal ions from the aqueous medium.

#### 3.6.2 FT-IR

Figure 4 displays the FT-IR spectra of GWNC before and after Cu(II) adsorption. These spectra showed a narrow and weak peak at between 3700 and 3200 cm<sup>-1</sup> attributed to the characteristic O-H stretching in alcohols, phenols, and carboxylic groups [44, 45]. The signals appearing at 2979 and 2903 cm<sup>-1</sup> were attributed to the stretching vibrations of asymmetric and symmetric C-H in methyl group [46]. The peak at 1584 cm<sup>-1</sup> belongs to the typical stretching vibration of the skeletal C=C in aromatic rings [47]. The signal at 1392 cm<sup>-1</sup> shows the C-H symmetrical bending from methyl groups or the -CH<sub>2</sub> scissoring vibration [48]. The relatively intense band observed at 1249 cm<sup>-1</sup> could be assigned to C-O-C stretching in ethers [49]. The band appearing at 1067 cm<sup>-1</sup> is C-O stretching peak in heterocyclic rings [50]. The signals at about 883 and 755 cm<sup>-1</sup> display C-H out-of-plane bending in an aromatic ring [51]. After Cu(II) loading, some variations occurred on the surface of GWNC. Figure 4 shows that many functional groups shifted to different frequency levels or disappeared after adsorption, indicating that the hydroxyl groups on the surface of GWNC are included in adsorbent-adsorbate interactions.

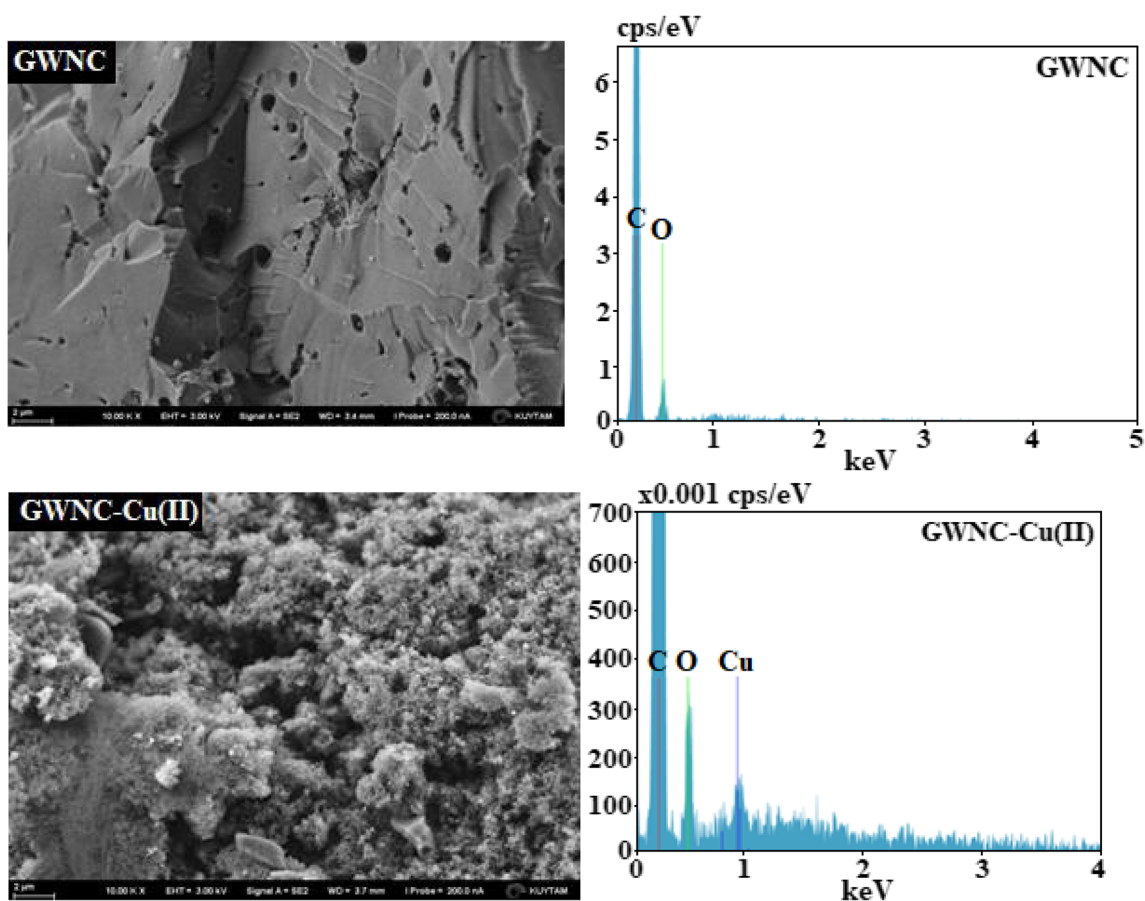


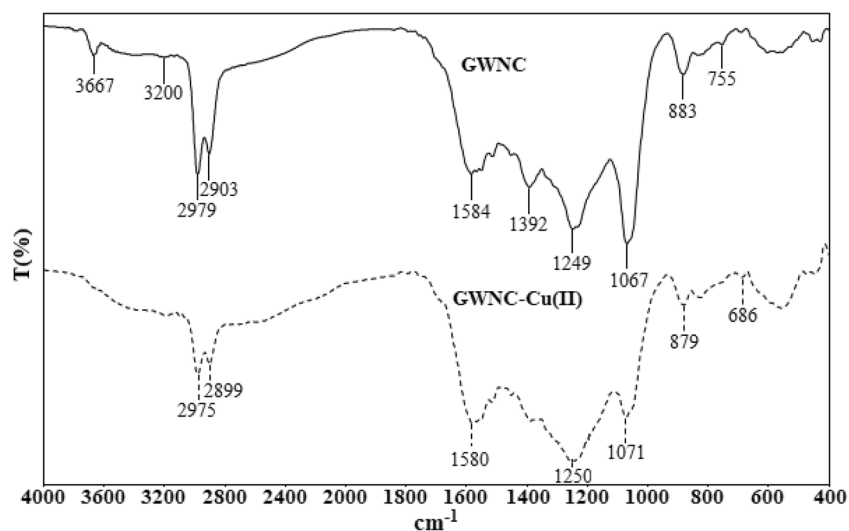
Fig. 3 SEM images and EDX spectra of GWNC before and after Cu(II) adsorption

### 3.6.3 XPS analysis

The XPS spectra of the GWNC sample with and without adsorbed Cu(II) ions are displayed in Fig. 5 a–c. It is clear that the existence of Cu  $2p$  peak in survey spectra for GWNC-Cu indicated that copper ions were adsorbed on the GWNC

surface [52]. Figure 5 c shows the high-resolution XPS spectra of Cu  $2p$  after adsorption were three peaks; Cu  $2p_{3/2}$  at 933.83 eV and two shake-up peaks at 941.5 and 953.2 eV can be observed [53]. These peaks are formed by the interaction between the hydroxyl groups and Cu(II) ions, which agreed with the result obtained from the FT-IR analysis [54].

Fig. 4 FT-IR spectra of GWNC before and after Cu(II) adsorption





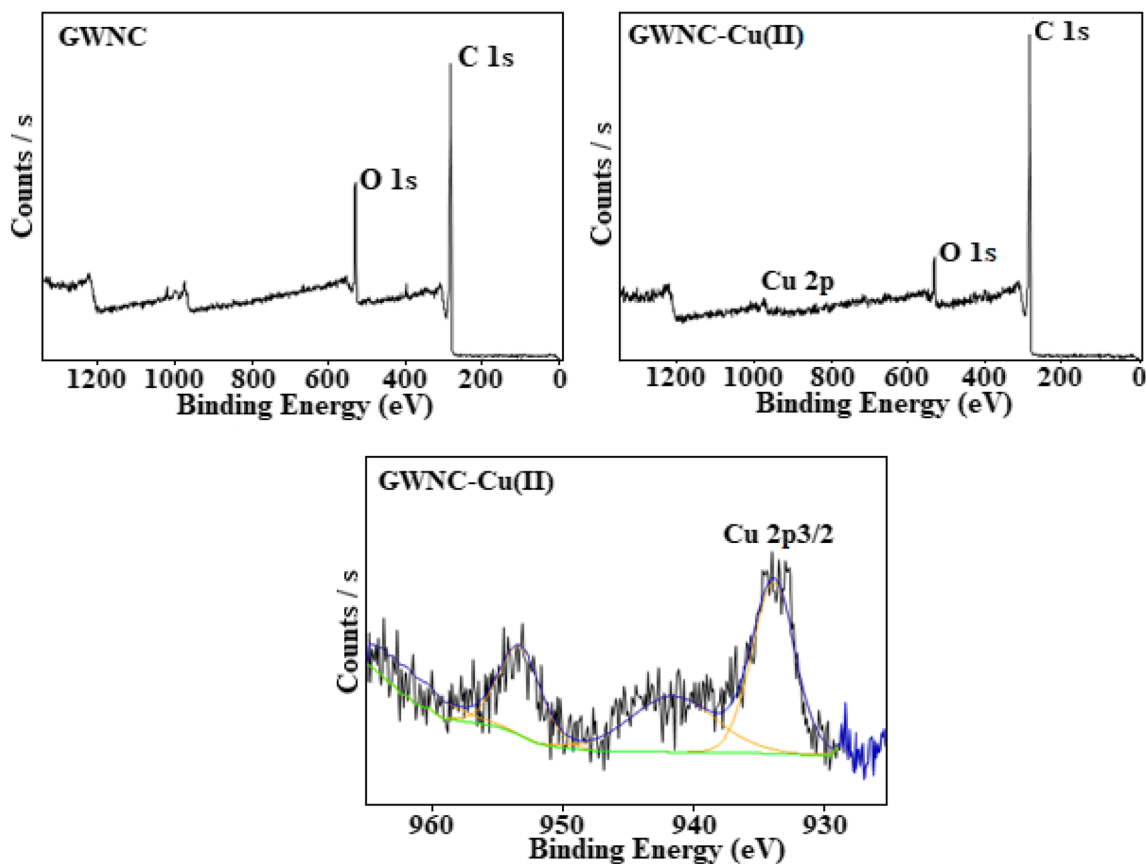


Fig. 5 The XPS spectra before and after adsorption and Cu 2p spectra after adsorption of the GWNC

### 3.7 Desorption and reusability

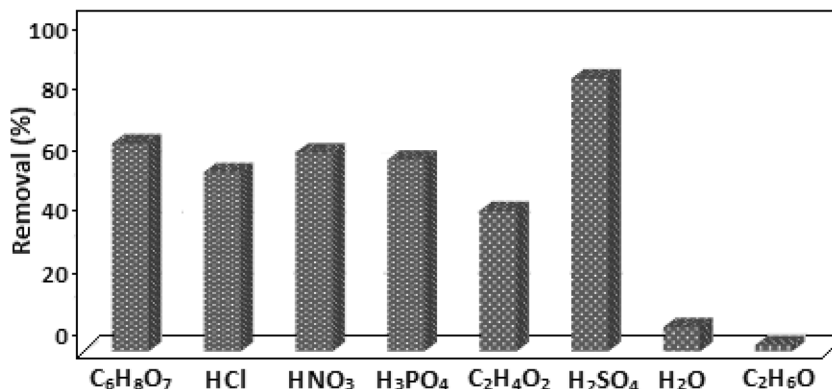
In this research, the desorption efficiency of Cu(II) with 0.1 mol L<sup>-1</sup> of various eluents (HCl, HNO<sub>3</sub>, H<sub>2</sub>SO<sub>4</sub>, H<sub>3</sub>PO<sub>4</sub>, CH<sub>3</sub>COOH, C<sub>2</sub>H<sub>6</sub>O, C<sub>6</sub>H<sub>8</sub>O<sub>7</sub>, and H<sub>2</sub>O) was investigated and is graphically presented in Fig. 6. As seen in this figure, the desorption yield of Cu(II) was 58.56% with HCl, 64.98% with HNO<sub>3</sub>, 89.14% with H<sub>2</sub>SO<sub>4</sub>, 62.64% with H<sub>3</sub>PO<sub>4</sub>, 45.94% with CH<sub>3</sub>COOH, 2.04% with C<sub>2</sub>H<sub>6</sub>O, 67.94% with C<sub>6</sub>H<sub>8</sub>O<sub>7</sub>, and 7.92% with H<sub>2</sub>O. The highest desorption yield of H<sub>2</sub>SO<sub>4</sub> is likely to cause the ion exchange of Cu(II) adsorbed to active

centers on the surface and the protons of sulfuric acid, which are more acidic than other desorption agents in water.

### 4 Conclusions

The removal amount of Cu(II) ions was found to increase with increasing solution pH, contact time, initial Cu(II) concentration, and temperature and to decrease with increasing GWNC dosage. The kinetic and equilibrium data were well obeyed by the pseudo-second-order kinetic and Langmuir isotherm models, respectively. The maximum adsorption capacity of

Fig. 6 Effect of various desorbing agents on desorption percentages of Cu(II) from GWNC (temperature, 298 K; time, 1 h; desorbent concentration, 0.1 M; GWNC dose, 0.1 g)



the GWNC measured to be  $80.0 \text{ mg g}^{-1}$  under optimized conditions of the solution pH of 5.0, GWNC dosage of 50 mg, contact time of 120 min, and solution temperature of  $50^\circ\text{C}$ . The adsorption mechanism was a very complex process, and intra-particle diffusion was not the only rate control step. The thermodynamic parameters determined for the Cu(II) adsorption process by GWNC showed that process was favored at higher temperature. The maximum desorption efficiency was observed as 89.14% with 0.1 M  $\text{H}_2\text{SO}_4$  solution.

**Funding information** This study received financial support from the Scientific Research Projects Coordinator of Dicle University (Grant No 12-ZEF-95).

## References

- Popuri SR, Frederick R, Chang CY, Fang SS, Wang CC, Lee LC (2014) Removal of copper (II) ions from aqueous solutions onto chitosan/carbon nanotubes composite sorbent. *Desal Water Treat* 52:691–701. <https://doi.org/10.1080/19443994.2013.826779>
- Hydari S, Shariffard H, Nabavinia M, Parvizi MR (2012) A comparative investigation on removal performances of commercial activated carbon, chitosan biosorbent and chitosan/activated carbon composite for cadmium. *Chem Eng J* 193–194:276–282. <https://doi.org/10.1016/j.cej.2012.04.057>
- Demiral H, Güngör C (2016) Adsorption of copper (II) from aqueous solutions on activated carbon prepared from grape bagasse. *J Clean Prod* 124:103–113. <https://doi.org/10.1016/j.jclepro.2016.02.084>
- Ghaedi AM, Ghaedi M, Irvani VA, Keshavarz N, Rad MM, Gupta VK (2015) Adsorption of copper(II) using modified activated carbon prepared from pomegranate wood: optimization by bee algorithm and response surface methodology. *J Mol Liq* 206:195–206. <https://doi.org/10.1016/j.molliq.2015.02.029>
- Ahmad R, Kumar R, Haseeb S (2012) Adsorption of  $\text{Cu}^{2+}$  from aqueous solution onto iron oxide coated eggshell powder: evaluation of equilibrium, isotherms, kinetics, and regeneration capacity. *Arab J Chem* 5:353–359. <https://doi.org/10.1016/j.arabjc.2010.09.003>
- Hu H, Zhang J, Lu K, Tian Y (2015) Characterization of *Acidosasa edulis* shoot shell and its biosorption of copper ions from aqueous solution. *J Environ Chem Eng* 3:357–364. <https://doi.org/10.1016/j.jece.2014.12.021>
- Cho HJ, Baek K, Jeon JK, Park SH, Suh DJ, Park YK (2013) Removal characteristics of copper by marine macro-algae-derived chars. *Chem Eng J* 217:205–211. <https://doi.org/10.1016/j.cej.2012.11.123>
- Kasnejad MH, Esfandiari A, Kaghazchi T, Asasian N (2012) Effect of pre-oxidation for introduction of nitrogen containing functional groups into the structure of activated carbons and its influence on Cu(II) adsorption. *J Taiwan Inst Chem Eng* 43:736–740. <https://doi.org/10.1016/j.jtice.2012.02.006>
- Xu C, Nasrollahzadeh M, Selva M, Issaabadi Z, Luque R (2019) Waste-to-wealth: biowaste valorization into valuable bio (nano) materials. *Chem Soc Rev* 48:4791–4822. <https://doi.org/10.1039/c8cs00543e>
- Ferjani AI, Jeguirim M, Jellali S, Limousy L, Courson C, Akrouit H, Thevenin N, Ruidavets L, Muller A, Bennici S (2019) The use of exhausted grape marc to produce biofuels and biofertilizers: effect of pyrolysis temperatures on biochars properties. *Renew Sust Energ Rev* 107:425–433. <https://doi.org/10.1016/j.rser.2019.03.034>
- Tangolar S, Turan M, Tangolar S, Ateş F (2019) Evaluation of amino acid contents and enzyme activities of seeds from Semillon and Carignane wine grape cultivars grown under different irrigation conditions. *Sci Hortic* 251:181–188. <https://doi.org/10.1016/j.scienta.2019.02.079>
- Portinho R, Zanella O, Feris LA (2017) Grape stalk application for caffeine removal through adsorption. *J Environ Manage* 202:178–187. <https://doi.org/10.1016/j.jenvman.2017.07.033>
- Saygılı H, Güzel F, Önal Y (2015) Conversion of grape industrial processing waste to activated carbon sorbent and its performance in cationic and anionic dyes adsorption. *J Clean Prod* 93:84–93. <https://doi.org/10.1016/j.jclepro.2015.01.009>
- Regmi P, García-Moscoso JL, Kumar S, Cao X, Mao J, Schafraan G (2012) Removal of copper and cadmium from aqueous solution using switchgrass biochar produced via hydrothermal carbonization process. *J Environ Manage* 109:61–69. <https://doi.org/10.1016/j.jenvman.2012.04.047>
- Wang XS, Qin Y (2005) Equilibrium sorption isotherms for  $\text{Cu}^{2+}$  on rice bran. *Process Biochem* 40:677–680. <https://doi.org/10.1016/j.procbio.2004.01.043>
- Jiang T, Liu W, Mao Y, Zhang L, Cheng J, Gong M, Zhao H, Dai L, Zhang S, Zhao Q (2015) Sorption behavior of copper ions from aqueous solution onto graphene oxide-CdS composite. *Chem Eng J* 259:603–610. <https://doi.org/10.1016/j.cej.2014.08.022>
- Zhang J, Li Y, Zhang C, Jing Y (2008) Adsorption of malachite green from aqueous solution onto carbon prepared from *Arundo donax* root. *J Hazard Mater* 150:774–782. <https://doi.org/10.1016/j.jhazmat.2007.05.036>
- Demirbaş E, Dizge N, Sulak MT, Kobya M (2009) Adsorption kinetics and equilibrium of copper from aqueous solutions using hazelnut shell activated carbon. *Chem Eng J* 148:480–487. <https://doi.org/10.1016/j.cej.2008.09.027>
- Shawabkeh R (2009) Equilibrium study and kinetics of  $\text{Cu}^{2+}$  removal from water by zeolite prepared from oil shale ash. *Process Saf Environ Protec* 87:261–266. <https://doi.org/10.1016/j.psep.2009.04.001>
- Lagergren S (1898) About the theory of so-called adsorption of soluble substance, *Kungliga Sven. Vetenskapsakademiens Handl* 24:1–39
- Ho YS, McKay G (1998) Kinetic models for the sorption of dye from aqueous solution by wood. *Process Saf Environ Prot* 76:183–191. <https://doi.org/10.1205/095758298529326>
- Weber WJ, Morris JC (1963) Kinetics of adsorption on carbon from solution. *J Sanit Eng Div ASCE* 89:31–60
- Güzel F, Saygılı H, Saygılı GA, Koyuncu F (2015) New low-cost nanoporous carbonaceous adsorbent developed from carob (*Ceratonia siliqua*) processing industry waste for the adsorption of anionic textile dye: characterization, equilibrium and kinetic modeling. *J Mol Liq* 206:244–255. <https://doi.org/10.1016/j.molliq.2015.02.037>
- Saygılı H, Güzel F (2015) Performance of new mesoporous carbon sorbent prepared from grape industrial processing wastes for malachite green and Congo red removal. *Chem Eng Res Des* 100:27–38. <https://doi.org/10.1016/j.cherd.2015.05.014>
- Sekulic MT, Boskovic N, Slavkovic A, Garunovic J, Kolakovic S, Papa S (2019) Surface functionalised adsorbent for emerging pharmaceutical removal: adsorption performance and mechanisms. *Process Saf Environ Protec* 125:50–63. <https://doi.org/10.1016/j.psep.2019.03.007>
- Langmuir I (1918) The adsorption of gases on plane surfaces of glass, mica and platinum. *J Am Chem Soc* 40:1361–1403. <https://doi.org/10.1021/ja02242a004>
- Freundlich H (1907) About the adsorption in solutions. *Z Phys Chem* 57:385–470
- Dubinín MM, Radushkevich LV (1947) The equation of the characteristic curve of activated charcoal. *Chem Zentr* 1:875–890

29. Hall KR, Eagleton LC, Acrivos A, Vermeulen T (1966) Pore and solid diffusion kinetics in fixed bed adsorption under constant pattern conditions. *Ind Eng Chem Fundam* 5:212–223. <https://doi.org/10.1021/i160018a011>
30. Bohli T, Ouederni A, Fiol N, Villaescusa I (2015) Evaluation of an activated carbon from olive stones used as an adsorbent for heavy metal removal from aqueous phases. *C R Chimie* 18:88–99. <https://doi.org/10.1016/j.crci.2014.05.009>
31. Erdem E, Karapinar N, Donat R (2004) The removal of heavy metal cations by natural zeolites. *J Colloid Interface Sci* 280:309–314. <https://doi.org/10.1016/j.jcis.2004.08.028>
32. Yavuz Ö, Altunkaynak Y, Güzel F (2003) Removal of copper, nickel, cobalt and manganese from aqueous solution by kaolinite. *Water Res* 37:948–952. [https://doi.org/10.1016/S0043-1354\(02\)00409-8](https://doi.org/10.1016/S0043-1354(02)00409-8)
33. Wu CH, Lin CF, Ma HW, His TQ (2003) Effect of fulvic acid on the sorption of Cu and Pb onto  $\gamma$ -Al<sub>2</sub>O<sub>3</sub>. *Water Res* 37:743–752. [https://doi.org/10.1016/S0043-1354\(02\)00391-3](https://doi.org/10.1016/S0043-1354(02)00391-3)
34. Zhang J, Fu H, Lv X, Tang J, Xu X (2011) Removal of Cu (II) from aqueous solution using the rice husk carbons prepared by the physical activation process. *Biomass Bioenergy* 35:464–472. <https://doi.org/10.1016/j.biombioe.2010.09.002>
35. Bouhamed F, Elouear Z, Bouzid J (2012) Adsorptive removal of copper (II) from aqueous solutions on activated carbon prepared from Tunisian date stones: equilibrium, kinetics and thermodynamics. *J Taiwan Inst Chem Eng* 43:741–749. <https://doi.org/10.1016/j.jtice.2012.02.011>
36. Li YH, Ding J, Luan Z, Di Z, Zhu Y, Xu C, Wei B (2003) Competitive adsorption of Pb<sup>2+</sup>, Cu<sup>2+</sup> and Cd<sup>2+</sup> ions from aqueous solutions by multi-walled carbon nanotubes. *Carbon* 41:2787–2792. [https://doi.org/10.1016/S0008-6223\(03\)00392-0](https://doi.org/10.1016/S0008-6223(03)00392-0)
37. An HK, Park BY, Kim DS (2001) Crab shell for the removal of heavy metals from aqueous solution. *Water Res* 35:3551–3556. [https://doi.org/10.1016/S0043-1354\(01\)00099-9](https://doi.org/10.1016/S0043-1354(01)00099-9)
38. Li M, Liu Q, Guo L, Zhang Y, Lou Z, Wang Y, Qian G (2013) Cu (II) removal from aqueous solution by *Spartina alterniflora* derived biochar. *Bioresour Technol* 141:83–88. <https://doi.org/10.1016/j.biortech.2012.12.096>
39. Khan TA, Mukhlif AA, E.A. (2017) Khan, Uptake of Cu<sup>2+</sup> and Zn<sup>2+</sup> from simulated wastewater using muskmelon peel biochar: isotherm and kinetic studies. *Egypt J Basic Appl Sci* 4:236–248. <https://doi.org/10.1016/j.ejbas.2017.06.006>
40. Zhang W, Li H, Kan X, Dong L, Yan H, Jiang Z, Cheng R (2012) Adsorption of anionic dyes from aqueous solutions using chemically modified straw. *Bioresour Technol* 117:40–47. <https://doi.org/10.1016/j.biortech.2012.04.064>
41. Ren Y, Li N, Feng J, Luan T, Wen Q, Li Z, Zhang M (2012) Adsorption of Pb (II) and Cu (II) from aqueous solution on magnetic porous ferrosin MnFe<sub>2</sub>O<sub>4</sub>. *J Colloid Interf Sci* 367:415–421. <https://doi.org/10.1016/j.jcis.2011.10.022>
42. Gao Y, Zhu X, Yue Q, Gao B (2018) Facile one-step synthesis of functionalized biochar from sustainable prolifera-green-tide source for enhanced adsorption of copper ions. *J Environ Sci* 73:185–194. <https://doi.org/10.1016/j.jes.2018.02.012>
43. Erdem A, Ngwabebhoh FA, Çetintaş S, Bingöl D, Yildiz U (2017) Fabrication and characterization of novel macroporous Jeffamine/diamino hexane cryogels for enhanced Cu(II) metal uptake: optimization, isotherms, kinetics and thermodynamic studies. *Chem Eng Res Des* 117:122–138. <https://doi.org/10.1016/j.cherd.2016.10.010>
44. Üner O, Bayrak Y (2018) The effect of carbonization temperature, carbonization time and impregnation ratio on the properties of activated carbon produced from *Arundo donax*. *Microporous Mesoporous Mater* 268:225–234. <https://doi.org/10.1016/j.micromeso.2018.04.037>
45. Bedin KC, Cazetta AL, Souza IPAF, Pezoti O, Souza LS, Souza PSC, Yokoyama JTC, Almeida VC (2018) Porosity enhancement of spherical activated carbon: influence and optimization of hydrothermal synthesis conditions using response surface methodology. *J Environ Chem Eng* 6:991–999. <https://doi.org/10.1016/j.jece.2017.12.069>
46. Liu X, He C, Yu X, Bai Y, Ye L, Wang B, Zhang L (2018) Net-like porous activated carbon materials from shrimp shell by solution-processed carbonization and H<sub>3</sub>PO<sub>4</sub> activation for methylene blue adsorption. *Powder Technol* 326:181–189. <https://doi.org/10.1016/j.powtec.2017.12.034>
47. Guo F, Li X, Jiang X, Zhao X, Guo C, Rao Z (2018) Characteristics and toxic dye adsorption of magnetic activated carbon prepared from biomass waste by modified one-step synthesis. *Colloids Surf A Physicochem Eng Asp* 555:43–54. <https://doi.org/10.1016/j.colsurfa.2018.06.061>
48. Fu K, Yue Q, Gao B, Wang Y, Li Q (2017) Activated carbon from tomato stem by chemical activation with FeCl<sub>2</sub>. *Colloids Surf A Physicochem Eng Asp* 529:842–849. <https://doi.org/10.1016/j.colsurfa.2017.06.064>
49. Rincón-Silva NG, Moreno-Pirajan JC, Giraldo L (2016) Equilibrium, kinetics and thermodynamics study of phenols adsorption onto activated carbon obtained from lignocellulosic material (*Eucalyptus globulus* Labill seed). *Adsorption* 22:33–48. <https://doi.org/10.1007/s10450-015-9724-2>
50. Gundogdu A, Duran C, Senturk HB, Soylok M, Imamoglu M, Onal Y (2013) Physicochemical characteristics of a novel activated carbon produced from tea industry waste. *J Anal Appl Pyrolysis* 104:249–259. <https://doi.org/10.1016/j.jaap.2013.07.008>
51. Mahmood T, Ali R, Naem A, Hamayun M, Aslam M (2017) Potential of used *Camellia sinensis* leaves as precursor for activated carbon preparation by chemical activation with H<sub>3</sub>PO<sub>4</sub>; optimization using response surface methodology. *Process Saf Environ Prot* 109:548–563. <https://doi.org/10.1016/j.psep.2017.04.024>
52. Qin L, Feng L, Li C, Fan Z, Zhang G, Shen C, Meng Q (2019) Amination/oxidation dual-modification of waste ginkgo shells as bio-adsorbents for copper ion removal. *J Clean Prod* 228:112–123. <https://doi.org/10.1016/j.jclepro.2019.04.249>
53. Sun XF, Hao Y, Cao Y, Zeng Q (2019) Superadsorbent hydrogel based on lignin and montmorillonite for Cu(II) ions removal from aqueous solution. *Int J Biol Macromol* 127:511–519. <https://doi.org/10.1016/j.ijbiomac.2019.01.058>
54. Li X, Deng G, Zhang Y, Wang J (2019) Rapid removal of copper ions from aqueous media by hollow polymer nanoparticles. *Colloid Surface A* 568:345–355. <https://doi.org/10.1016/j.colsurfa.2019.02.033>

**Publisher's note** Springer Nature remains neutral with regard to jurisdictional claims in published maps and institutional affiliations.